# Electric Fenton technology with *Jacaranda* fruit shell biochar as particle electrode for the removal of emerging pollutant ciprofloxacin hydrochloride

**Yuqin Liu[1], Yu Shi[1], Yongqiang Liu[2], Ailin Fan[1], Bo Xu1[†], Haiyan Qiu[1], Guihong Lan[1], Ming Zhang[3]**

[1]*College of Chemistry and Chemical Engineering, Southwest Petroleum University, No 8 Xindu Avenue, Sichuan, Chengdu 610500, China*
[2]*Faculty of Engineering and Physical Sciences, University of Southampton, Southampton SO17 1BJ, UK*
[3]*China Railway Water Group Co., Ltd., Xi'an 710000, China*

**ABSTRACT**

The overuse of antibiotics has become a serious environmental problem, and addressing how to remove antibiotics from aquatic environments poses a significant challenge. This study prepared a porous biochar material (BSJ) using natural Jacaranda fruit shells as raw materials and combined it with an electric Fenton system (EF-BSJ) to degrade ciprofloxacin hydrochloride (CIP). Characterization and analysis of biochar using SEM, BET, Raman spectroscopy, and other methods revealed that the porous structure and aromatic functional groups of biochar play a crucial role in adsorbing CIP. The effects of carbonization temperature and carbonization time on the adsorption of CIP by biochar were investigated during the biochar preparation process. At 800°C and 1.5 hours, the maximum adsorption efficiency of biochar for CIP is 96.88%. In addition, thestudy investigated the impact of cathode and anode materials of the EF-BSJ system on the degradation efficiency of CIP. When platinum-titnium plating was used as the anode and foam nickel electrode as the cathoded, the CIP removal rate could reach 95.48%. Finally, the UV full-band scanning method was used to determine that CIP was degraded into small molecule substances, achieving the goal of removing CIP. This study introduces a novel strategy for eliminating antibiotics.

**Keywords:** Adsorbed, Biochar chemical properties, Biochar contaminates, Biochar physical properties, Biomass, Ciprofloxacin hydrochloride

## Graphical Abstract

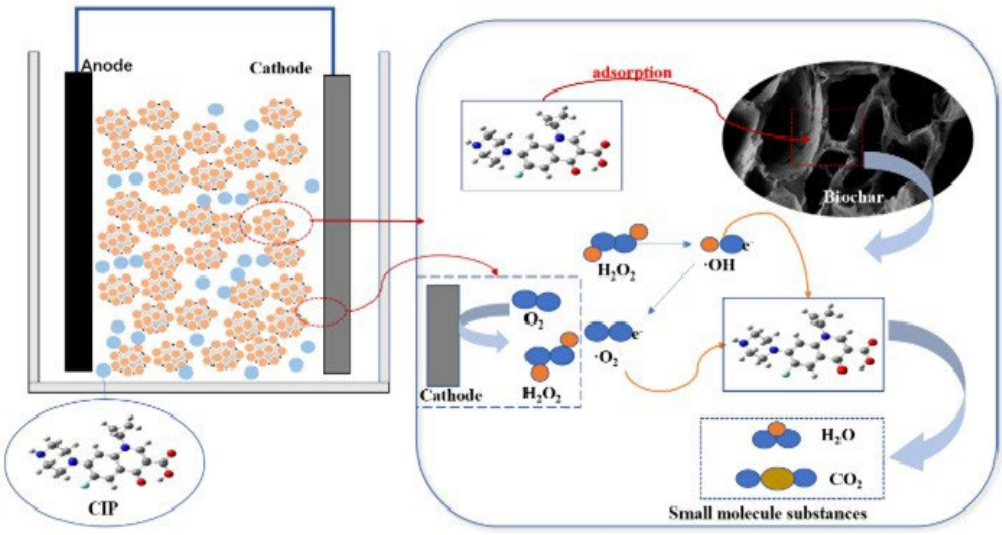

## 1. Introduction

In the last few years, due to the excessive use of antibiotic drugs, fluoroquinolones have been frequently detected in aquatic environments [1]. Ciprofloxacin hydrochloride (CIP), a typical fluoroquinolone antibiotic, has attracted widespread attention as an emerging pollutant due to its high ecological toxicity [2]. However, conventional wastewater treatment technologies struggle to remove CIP due to its persistence [3, 4]. In the last few years, carbon-based materials such as biochar have received increasing attention as adsorbents for adsorbing antibiotics in wastewater treatment due to their low-cost and easy availability of raw materials. Biochar has an extremely high specific surface area and surface functional groups; therefore, it exhibits excellent adsorption performance [5]. Recently, extensive research has been conducted to increase the number of functional groups on the surface of biochar through chemical modification [5, 6], or by optimizing pyrolysis conditions to enhance the adsorption capacity of biochar. Active groups in biomass, however, are easily lost during the high-temperature pyrolysis process, which reduces the adsorption capacity of biochar [7]. According to research by Cheng et al., lignin possesses numerous active functional groups and specific chemical reactionsites, enabling the modification of necessary functional groups. Therefore, biochar prepared from lignin possesses physical and chemical adsorption characteristics, making it suitable for reducing organic pollutants, heavy metals, dyes and other pollutants [8].The *Jacaranda* fruit shell, a natural lignin porous material, offers sigifi- cant advantages in biochar preparation. Treviño-Cordero et al. reported that *Jacaranda* biochar can be used to remove AB25, methylene blue dyes, and the heavy metal $Pb^{2+}$ [9]. However, it is unclear if pyrolysis conditions affect the characteristics of *Jacaranda* biochar and consequently impact pollutant removal. Therefore, this study investigated the preparation of biochar from

the shell of *Jacaranda* fruit and its adsorption capacity for dyes, antibiotics, and heavy metals.

The adsorption capacity of biochar for removing pollutants has been demonstrated.However, the lack of available methods to de- sorb the adsorbents for biochar reuse or manage the pollutant-satu- rated adsorbents has raised environmental concerns [10]. In light of this, some researchers combined biochar with oxidation to de- grade the adsorbed pollutants. According to the investigation by Sirés et al., the electrochemical advanced oxidation process (EAOP) has emerged as a promising method for sewage treatment to elimiate a wide variety of organic pollutants [11]. The EAOP uses highly reactive hydroxyl radicals to oxidize organic pollutants [11]. When biochar is combined with electric Fenton, hydroxyl radicals pro- duced from electric Fenton can fully oxidize pollutants adsorbed by biochar and thus regenerate biochar for adsorption in situ [12]. Traditional two-dimensional electric Fenton systems, however, cannot fully utilize •OH radicals due to low current density, result- ing in low efficiency and a short service life [13]. Recently, re- searchers have significantly enhanced the processing capacity and current efficiency of the electric Fenton system (EF) by incorporat- ing particle electrodes, such as metal particles or carbon aerogel [14]. Under an external electric field, particles can be easily polar- ized to form charged microelectrodes. This shortens the distance between pollutants and electrodes, enhancing mass transfer effi- ciency, and consequently improving electrolysis efficiency [15]. Biochar is a cost-effective and environmentally friendly material that can serve as a combination of adsorbent and catalyst in electric
Fenton systems [16].

This study aimed to develop a three-dimensional electric Fenton system using *Jacaranda* fruit shell biochar (EF-BSJ) derived from natural lignin porous materials as a particle electrode for the degra- dation of CIP. Three representative pollutants, including anti- biotics, dyes, and heavy metals, were investigated to study the effects of pyrolysis conditions on the adsorption of biochar and its adsorption mechanism. The effectiveness of the bio- carbon-electric Fenton system in treating pollutants was evaluated using the antibiotic CIP.

## 2. Materials and Methods

### 2.1. Materials and Chemicals

The shell of *Jacaranda* fruit collected from the greening arbor of Southwest Petroleum University in Sichuan Province, China, was washed, crushed, and screened to a specific size of 50 meshes. It was dried to a constant weight in an 80°C oven before further use. Ciprofloxacin hydrochloride, tetracycline, Congo red, Methyl orange, and other chemical reagents were all obtained from Chengdu Huaxia Chemical Reagent Co., Ltd. (Sichuan, China). Other chemicals used in this study were all of analytical grade (AR ≥ 98%). If there was no specific description, they were all purchased from Kelong Chemical. All solutions were prepared with deionized water.

### 2.2. Preparation of Biochar by Pyrolysis

The biomass from the shell of Jacaranda fruit was prepared by pyrolysis after being pretreated in the initial step. Firstly, place the constant weight biomass into a grinder to crush it into small particles, and then screen out particles with a size smaller than 5 mesh. Then, place the particles with a particle size smaller than 5 mesh into a nickel crucible and carbonize them in a tube furnace (with aheating rate of 10 °C/min). crush them into small particles and screen out particles with a particle size of less than 5 mesh. Then, put the particles with particle size less than 5 mesh into a nickel crucible and carbonized them in tube furnace (the heating rate is 10 °C/min). Screened out carbonized biochar particles with a diameter less than 0.25 mm from the carbonized biochar particles. After ultrasonic cleaning and drying, *Jacaranda* shell biochar (BSJ) was obtained. Added 100 mL of concentrated nitric acid (6 mol/L) to 4 g of carbonized biochar particles and soaked them in a shaker at 25°C and 200 rpm for 8 hours. Then, wash the biochar with dilute hydrochloric acid (0.1 mol/L), sodium hydroxide (0.1 mol/L), and deionized water until it reaches a neutral pH. Finally, put the washed biochar particles into an 80°C oven and bake them until a constant weight is achieved to obtain activated biochar particles.

### 2.3. Electrochemical Apparatus and Operating Procedures

The design diagram of the experimental device is shown in Fig. S1 of the supplementary materials, which consiste of a DC power supply, an air pump, an anode plate (platinum-plated titanium electrode), a cathodeplate (foam nickel), and a magnetic rotor. The working volume of the device used in this study is 65 mm
× 65 mm × 70 mm. The anode and cathode were placed in parallel in the device with a distance of 45mm between them. At a distance of 10 mm from the wall, the middle was evenly filled with carbon- ized particles saturated with adsorption. While the aeration pipe continuously replenished dissolved oxygen into the solution, a magnetic stirrer was placed in the reactor and stirred continuously

at a temperature of 20℃. It is worth noting that all experiments were carried out at a temperature of 20℃ and repeated three times to obtain the average value. Unless otherwise specified, the concen- tration of the CIP solution involved in this study was 100 mg/L.

## 2.4. Morphological and Compositional Characterization of Biochar

C, H, O, N, and S elements in *Jacaranda* shell fruit were analyzed by an elemental analyzer (Elemantar Vario UNICUBE, Germany). At a constant heating rate of 100 ℃/min to reach a temperature of 900℃, 2.5 grams of *Jacaranda* shell fruit were introduced into a thermogravimetric analyzer. After incubation for 25 minutes, the elemental composition of blue flower fruit shells was measured. The morphology of the materials was observed using scanning electron microscopy (SEM, SU 3500, China). The specific surface area of BSJ was measured using the automatic specific surface area and pore analyzer (BET, ASAP 2460, U.S.A.). The functional groups of biochar were analyzed using an automatic Raman spec- trometer (ID Raman micro IM-52, Chain). Thermogravimetric anal- ysis was used to analyze the biomass composition (TGA SDTA851, Switzerland). Anultraviolet-visible spectrophotometer was used to determine the concentration of CIP and degraded small analytical substances (UV-1800, China). In this study, the cellulose content was determined using nitric acidand acetic acid-potassium dichro- mate method, following the procedures outlined in the literature. The hemicellulose content was determined through calcium nitrate iodimetry, while the lignin content was assessed using the acetic acid-potassium dichromate method [17]. All characterizations in this study were conducted using biochar prepared at the optimal carbonization temperature and time.

## 2.5. Efficiency Evaluation of BSJ and BSJ-EF

Heavy metal, dye, and antibiotic pollutants (CIP) were used to assess the adsorption performance of BSJ, while the degradation efficiency of CIP was employed to evaluate the performance of the electric Fenton system. Firstly, based on the experimental results of BSJ carbonization time and carbonization temperature mentioned above, the optimal carbonization temperature and time were selected. The initial concentrations and adsorption times of various pollutants are shown in supplementary material Table S1. below. Antibiotics and dyes were analyzed using UV-visible spectrophotometry to measure the absorbance of each substance. The concentration of antibiotics and dye pollutants was then calcu- lated based on standard curves. The heavy metal levels were de- termined using flame atomic absorption spectrophotometry, and the concentration of pollutants in each filtrate was calculated based on a standard curve.

To construct an effective three-dimensional electric Fenton sys- tem, various cathode materials such as foam nickel, activated car- bon fiber, and porous graphite plate, as well as and anode electrode materials including platinum-plated titanium electrode, iri- dium-ruthenium electrode, and Sb-doped $SnO_2$/Ti electrode, were evaluated in degradation experiments using CIP as the only pollutant. The reaction conditions were controlled as follows: CIP concentration of 20 mg/L, reaction volume of 200 mL, cell voltage of 10 V, current of 1 A, $Fe^{2+}$dosage of 4 mmol/L, NaSO4 dosage

of 0.2 mol/L, aeration intensity of 250 mL/min, biochar particles dosage of 3 g, and agitator speed of 300 r/min. After a 30-min reaction, 1 mL of the reaction solution was extracted, followed by membrane filtration with a 0.22 μm pore size. The filtrate was analyzed using an ultraviolet spectrophotometer to measure the absorbance of the solution at 276.5 nm. Refer to the standard "Determination of Chemical Oxygen Demand in Water Quality
- Rapid Digestion Spectrophotometry" (HJ/T 399-2007) and utilize the digester (LB-901B) and visible spectrophotometer (V-1800) to measure $COD_{Cr}$ in the solution.

Finally, to confirm the degradation of CIP by EF-BSJ, a UV full-band scanning method was employed to analyze the changes in functional groups before and after degradation. After 60 minutes of reaction, take 1 mL of solution from the reaction tank and pass it through a 0.22 μm filter membrane. Subsequently, ultraviolet scanning is conducted within the wavelength range of 200~400 nm. At the same time, the original solution before degradation is also scanned across the full spectrum.

Eq. (1) was used to evaluate the adsorption performance of coupled biochar and electric Fenton system.

$$\eta=[(C_0-C)\times 100\%]/C_0 \quad (1)$$

where:

$\eta$: Adsorption removal rate of contaminants, %;

$C_0$: The initial concentration of contaminants, mg/L;

C: The concentration of contaminants after treatment, mg/L.

### 2.6. Dynamic Model

In order to study the adsorption mechanism of antibiotics by the BSJ, the pseudo first order kinetic model shown in Eq. (2) and pseudo second order kinetic model shown in Eq. (3). Tow models were used to fit the experimental data, respectively [18].

$$\ln(Q_e-Q_t)=\ln Q_e-k_1 t \quad (2)$$

$$t/Q_t=1/(k_2 Q_e^2)+t/Q_e \quad (3)$$

where:

and : the adsorption capacities at equilibrium, mg/g;

and : the pseudo first-order and pseudo-second-order rate con- stants, respectively, g/mg·min;

: the adsorption time, (min).

## 3. Results and Discussion

### 3.1. Compositional, Thermal, and Morphological Characterization of BSJ

#### 3.1.1. Element analysis of biochar

The organic element analyzer conducted elemental analysis on the shell of *Jacaranda* fruit, and the results are shown in supplementary material Table S2. The carbon content of the shell of the *Jacaranda* fruit increased from 45.12% to 80.79%. The higher the carbon content, the greater the porosity and specific surface

area of the biochar formed [19]. Through the aforementioned ex- perimental methods, it was determined that the lignin content in the shell of *Jacaranda* fruit was 34.62%, while cellulose and hemicellulose were 25.60% and 19.51%, respectively. The higher the content of lignin in biomass, the more stable the structure of biochar formed [20]. At the same time, cellulose and hemi- cellulose will undergo pyrolysis to form carboxyl, hydroxyl, and other alkaline functional groups, enhancing the adsorption capacity of biochar [20].

### 3.1.2. Thermogravimetric analysis

The thermogravimetric analysis results of the shell of *Jacaranda* fruit are shown in Fig. S2 of the supplementary materials. In the first stage, the temperature ranges from 0℃ to 141.3℃, which corresponds to the evaporation of water from the shell of the *Jacaranda* fruit, resulting in a weight loss of only 0.976%. In Stage II, the temperature range was 196.30℃ to 503.64℃, leading to a weight loss of approximately 72.62% in the shell of the *Jacaranda* fruit. During this stage unstable organic matter decomposed, con- stituting the primary component of pyrolysis. In the third stage, the temperature ranged from 503.64℃ to 900℃, and the mass loss of the shell of the *Jacaranda* fruit was about 5.14%. This stage involved the mass loss of refractory organic matter and ash [9]. At 900℃, the residual mass value after the carbonization of biochar was 21.27%, representing the yield of the produced biochar.

### 3.1.3. SEM morphology

Fig. 1 displays the SEM results of native biomass and Jacaranda fruit biochar. Among them, Figs. 1 (a1) and (b1) show the results obtained at a magnification of 1000 times, while Figs. 1 (a2) and 1 (b2) depict the results obtained at a magnification of 4000 times. From Fig. 1 (a), it can be seen that the shell structure of the native Jacaranda fruit was loose, with many irregular hollow channels. The pore diameter was mainly concentrated in the meso- porous range (<20 nm). From Fig. 1 (b), it can be seen that after modification with nitric acid, the ash content in the pores of the Jacaranda fruit shell disappears, and the pore structure is exposed on the surface, making the pore structure more regular. The BET measurement results showed that the surface area of the shell of Jatropha japonica was 392 $m^2/g$. After pyrolysis, the surface area of the shell biochar increased to 570 $m^2/g$.

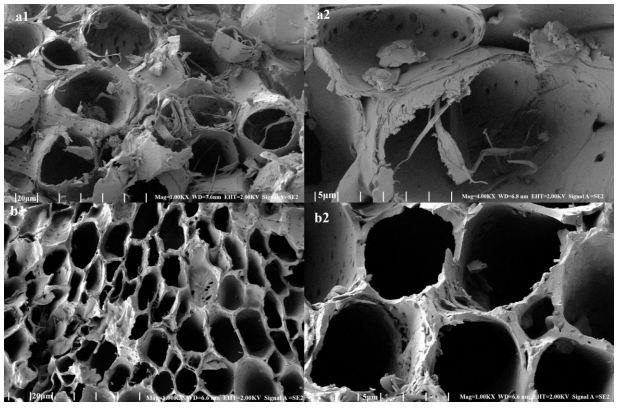


**Fig. 1.** SEM (a) Biomass (b) Biochar.

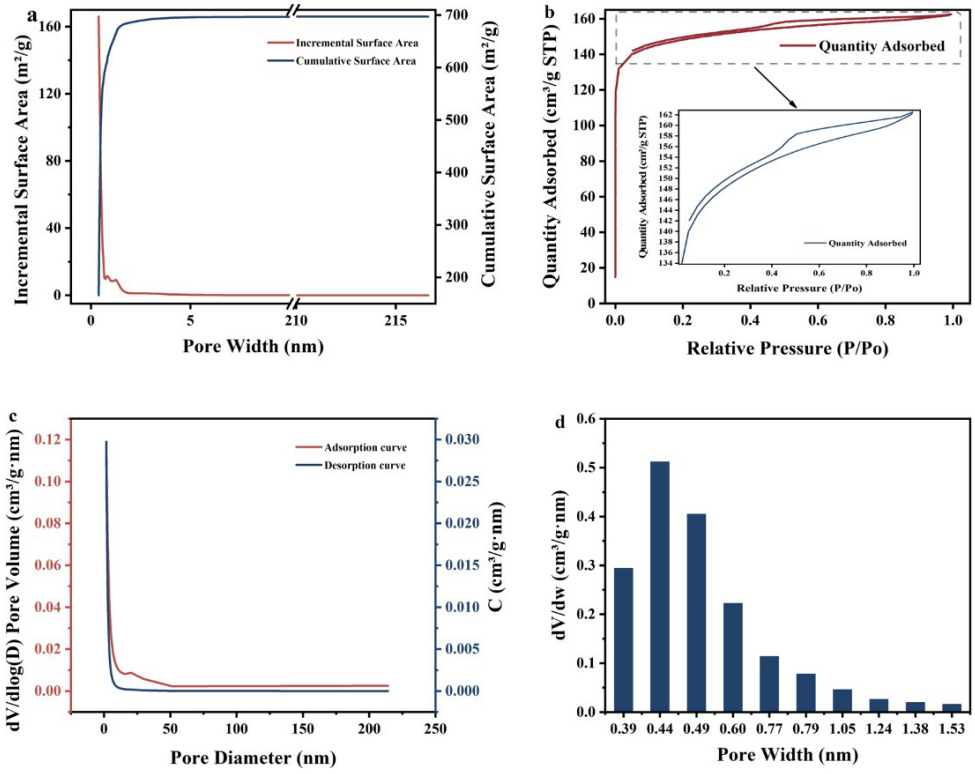


**Fig. 2.** BET analysis. (a) surface area integration (b) Isothermal adsorption desorption curve (c) BJH Adsorption and Desorption Curve of Biochar (d) HK Curve of Biochar.

### 3.1.4. BET detecting

In order to further investigate the changes in surface area and porosity of *Jacaranda* fruit biochar, the BJH and BET methods were used to characterize and analyze the biochar samples. The average pore diameter and pore volume of the biochar after activa- tion are calculated using the BJH model, and the results are shown in supplementary material Table S3. The specific surface area of activated biochar was 699.55 $m^2/g$, the average pore diameter was 1.75 nm, and the pore volume was 0.25 $cm^3/g$, which was higher than that of inactivated biochar. This demonstrates that the nitric acid treatment of biochar effectively disrupts the dense structure of cellulose along with its intramolecular and inter- molecular hydrogen bonds. This process increases the specific surface area of biochar and creates a porous structure, providing more active sites [5].

From Fig. 2 (a), it can be seen that the increase in the surface area of biochar was mainly concentrated within 5 nm. The experimental results indicate that the larger specific surface area of biochar is attributed to the well-developed microporous structure of the prepared biochar. The pore size distribution range of biochar can be determined from the BJH adsorption-desorption curve. It is worth noting that there was a hysteresis loop in the nitrogen desorption isotherm of BSJ (Fig. 2 (b)). This indicates the presence of mesopores in BSJ [21]. It can be observed from Fig. 2 (c) that the primary pore size distribution range of the biochar derived from the shell of the *Jacaranda* was less than10 nm. The main

pore size distribution of biochar can be obtained by the calculation of the HK equation [14]. According to the activated biochar HK curve (Fig. 2 (d)), the concentrated of micropores in the biochar was highest at 0.45 nm. According to the study by Li et al., the pore size of BSJ is less than 2 nm because the raw material used to prepare biochar in this study contains a significant amount of cellulose [22]. The primary pore size distribution of the prepared BSJ is 0.45 nm, which is the main reason for its strong absorption capacity and high surface area [23]. The specific surface area and pore volume facilitate the infiltration of pollutants into the pores, while a high specific area can offer sufficient enough adsorption sites to adsorb pollutants [24].

### 3.1.5. Raman analysis

The Raman spectrum of biochar from the shell of *Jacaranda* fruit is presented in Fig. S3 of the supplementary materials. The biochar from the shell of *Jacaranda* fruit exhibited prominent peaks in the D band at 1351.90~1358.50 $cm^{-1}$, attributed to the presence of aromatic carbon rings [25]. There were also clear peaks in the G band ranging from 1600.70 to 1603.20, which were attributed to the tangential stretching vibration between carbon atoms [12]. The $I_D/I_G$ ratio of activated biochar shown in Fig. S3 was 2.23, while the $I_D/I_G$ ratio of activated biochar was 2.05. There is no significant difference in Raman spectra between activated and deactivated biochar, indicating that activation has no effect on the structure of biochar.

### 3.1.6. Zeta potential analysis

The change in solution pH value will affect the surface charge of biochar. When the solution pH value is less than the zero-charge point, the biochar surface is positively charged, which is conducive to the adsorption of anions. When the pH value of the solution is greater than the zero-charge point, the surface of biochar is negatively charged, which is favorable for cation adsorption. The experiment analyzed the isoelectric point of the biochar based on the shell of the jacaranda using zeta potential detection. The isoelectric point, $pH_{pzc}$ = 4.99, can be observed in Fig. S4 of the supplementary materials.

## 3.2. Optimization of Pyrolysis Conditions for The Preparation of Biochar

Temperature is one of the most important factors that affect bio- char's characteristics. Many studies have shown that as the carbonization temperature increases, the specific surface area of biochar formation increases by about an order of magnitude [26-28]. According to the pyrolysis results of TGA, the weight loss of biochar remains relatively constant when the carbonization temperature ranges from 400℃ to 800℃. The properties of biochar at this stage are relatively stable, which is conducive to the adsorption of pollutants by biochar. This study explored the pyrolysis temper- atures of 500℃, 600℃, 700℃, and 800℃. Adsorption rates of CIP by char at temperatures ranging from 500 to 800℃ were 32.14%, 47.05%, 63.68%, and 87.79%, as illustrated in Fig. 3 (a). The en- hanced CIP adsorption by char from high temperatures may be attributed to the increased decomposition of organic substances at higher temperatures, leading to further enhancement of the pore structure of biochar. The decomposition of organic matter allows biochar to have a larger pore volume, specific surface area, and adsorption sites [29].

Another important factor that affects the formation of the pore structure of biochar is the duration of pyrolysis. It was reported that increasing the pyrolysis duration promoted the disintegration of cellulose and lignin in BSJ, leading to the changes in pore structure of biochar and an increase in adsorption sites [30]. The adsorption rates of CIP by char were 87.79%, 96.88%, and 96.99% respectively, with pyrolysis durations of 1 hour, 1.5 hours, and 2 hours at 800℃ (Fig. 3 (b)). The adsorption rates of CIP by charcoal reached stability when the pyrolysis duration exceeded 1.5 hours.

This is mainly because a prolonged carbonization time affects the physical, chemical properties, and surface structure of biochar [31]. Long pyrolysis duration at high temperatures might destroy the functional groups of biochar, resulting in a decrease in the affinity of biochar to pollutants. Consequently, this led to a decrease in the adsorption rate of biochar [32]. At the same time, long pyrolysis duration at high temperatures might reduce the oxy- gen-containing functional groups of biochar, as well as the types and quantities of surface functional groups, ultimately weakening the adsorption rate of biochar [33]. According to the results, 800°C and 1.5 hours were selected as the optimal pyrolysis conditions for the preparation of biochar.

## 3.3. Pollutant Adsorption by Biochar

### 3.3.1. Dye adsorption by BSJ

In this study, four dyes, including anionic dyes like methyl orange and Congo red, and cationic dyes such as methylene blue and rhodamine B, were utilized to assess the dye adsorption capacity of *Jacaranda* biochar and investigate its removal mechanism. The experimental results are shown in Fig. 4 (a). It can be seen that the adsorption capacity of BSJ for methylene blue was 374.59 mg/g; followed by Methyl orange at 249.59 mg/g, Rhodamine at
99.25 mg/g, and Congo red at 66.39 mg/g. The highest adsorption rate of BSJ prepared in this study for dyes is 99%. This is because BSJ has a natural porous structure, which helps to significantly improve the adsorption capacity and rate of dyes [25].

From the above experimental results, it can be seen that the adsorption capacity of BSJ for cationic dyes was greater than that for anionic dyes. The BET analysis indicates that BSJ, after nitric acid activation, exhibits a more developed pore structure and a larger specific surface area. The Raman spectrum shows that the activated BSJ has more acidic oxygen functional groups. These factors increase the affinity between BSJ and cationic dyes [20]. On one hand, the zero charge point of biochar activated by nitric acid was less than 7. In the solution with pH of 9, the surface of biochar is negatively charged, and positively charged cations are absorbed by electrostatic attraction [34]. On the other hand, activated biochar has a well-developed pore structure that allows dye molecules with relatively small mass diffuse freely within the pores [35]. The molecular weights of the cationic dyes methyl-

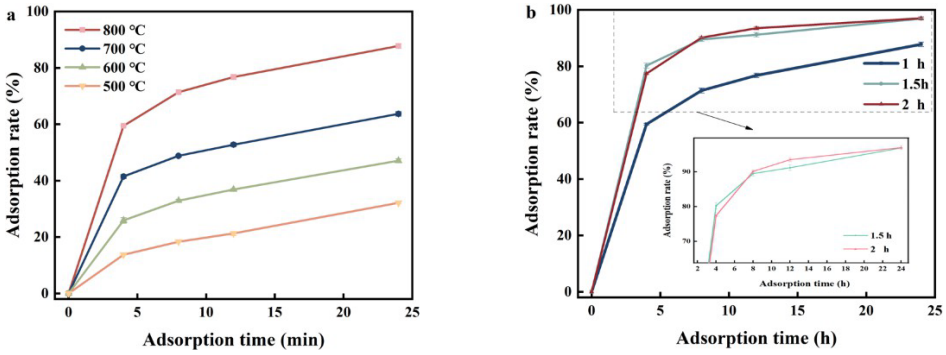


**Fig. 3.** Changes in the adsorption rate of CIP by Char from different pyrolysis temperatures (a) Effect of pyrolysis temperature on the adsorption rate of ciprofloxacin hydrochloride (b) Effect of pyrolysis duration on the adsorption rate of ciprofloxacin hydrochloride.

ene blue and Rhodamine B are 319.85 and 479.01, respectively. In contrast, the molecular weights of the anionic dyes Methyl orange and Congo red are 696.66 and 327.33, respectively. Therefore, the adsorption rate of cations on BSJ is higher than that of anions.

### 3.3.2. Adsorption of heavy metals by BSJ

The adsorption results of biochar on four heavy metal ions (Pb, Cu, Cd, Zn) are shown in Fig. 4 (b). The results showed that the adsorption quantity of Pb was 58.47 mg/g, which was the highest, followed by Cd with an adsorption capacity of 49.81 mg/g, Cu with an adsorption quantity of 25.70 mg/g, and Zn with an adsorption effect only 14.19 mg/g.

Based on the Raman spectrum analysis, the surface of biochar after nitrification and oxidation activation contains a large number of different kinds of acidic oxygen-containing functional groups. These groups can promote the ion exchange reaction between heavy metal ions and BSJ [36]. BSJ's heavy metal ions will undergo precipitation and complexation reactions with the heavy metal ions in the solution, thereby reducing the concentration of heavy metals in the solution. According to the Zeta potential, when the pH of the solution is 7, the BSJ surface becomes negatively charged. This charge enables the removal of positively charged heavy metal ions from the water through electrostatic adsorption. According to the BET analysis, it was found that the porosity of BSJ is relatively high, which can facilitate the entry of heavy metals into the air voids for physical adsorption. In summary, the adsorption of heavy metal ions in water by BSJ is achieved through electrostatic inter- actions, ion exchange, physical adsorption, and other processes.

The specific surface area, number of surface-active functional groups, and cation exchange capacity of biochar determine its adsorption activity for heavy metals [37].

### 3.3.3. the adsorption of antibiotics by BSJ

To explore the adsorption potential of BSJ to antibiotics, four typical antibiotics (e.g., ciprofloxacin, ampicillin, roxithromycin, tetracycline) were tested in the experiment. As shown in Fig. 4 (c), the adsorption capacity of BSJ for all types of antibiotics showed little difference, ranging from 6to7 mg/g. The adsorption rate of BSJ for four types of antibiotics was over 90%, with a 99% adsorption rate for CIP.

The adsorption of antibiotics on BSJ is a result of physical and chemical interactions [38, 39]. Physical adsorption is primarily attributed to pore adsorption. Both SEM and BET results demonstrate that BSJ has a high specific surface area and a rich pore structure, which facilitates the diffusion of antibiotic molecules into its pores and inner surface from the solution for adsorption. The Raman spectroscopy results indicate that BSJ contains a large number of oxygen-containing functional groups, mainly carboxyl and hydroxyl groups. Hydroxyl and carboxyl groups form hydrogen bonds with oxygen (O) and nitrogen (N) in anionic antibiotics, leading to the adsorption of antibiotics from aqueous solutions through hydrogen bonding. Due to differences in the molecular weight of antibiotics and limitations in the type and quantity of functional groups in BSJ, the adsorption capacity of BSJ for the four antibiotics varies slightly.

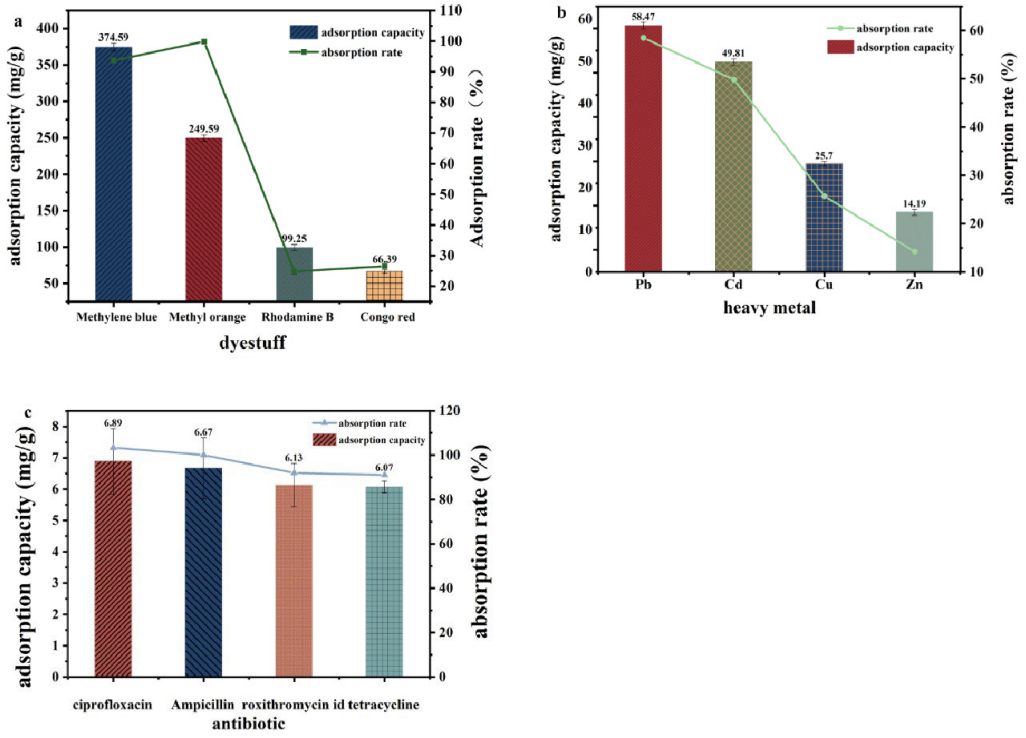


**Fig. 4.** The adsorption capacity and adsorption rate of BSJ for different pollutants (a) Adsorption of dye by BSJ (b) Adsorption of heavy metals by BSJ (c) Antibiotic adsorption by BSJ.

### 3.4. Dynamic Model Analysis

Pseudo first-order and pseudo-second-order models are two com- mon models used to study adsorption kinetics. Fig. S5 of the supplementary materials displays the fitting results of the two dynamic models, while supplementary material Table S4. presents the dynamic parameters of the two models. Compared with $R^2$ values ranging from 0.87 to 0.94 for the pseudo-first order model, the pseudo second-order model is more appropriate for fitting experimental data, with $R^2$ values ranging from 0.92 to 0.99. In addition, the calculated equilibrium adsorption capacity (Qe) of 90.334 mg/g based on the pseudo-second-order model is closer to the experimental adsorption amount of 87.795 mg/g. This shows that the pseudo second-order kinetic model is more suitable for simulating the adsorption of antibiotics by the biochar of the *Jacaranda*. As shown in Table S4., the Qe increased gradually as the temperature rose, indicating that the carbonization temperature positively influenced the adsorption of CIP by BSJ. On the contrary, the adsorption rate constant $K_2$ indicates that the adsorption of CIP by BSJ is dominated by slow adsorption. The results of the study revealed the chemical adsorption characteristics of the BSJ to antibiotics.

### 3.5. Screening of Cathode and Anode Materials for Three- Dimensional Electric Fenton System

Different anodes have speciffic effects on the three-dimensional electrochemical degradation of CIP. Fig. 5 (a); Fig. 5 (b) shows a comparative study of the degradation and removal efficiency of CIP and COD in wastewater using different electrodes. The experimental results show that the electrochemical degradation of CIP with a platinum-plated titanium electrode as the anode

was more effective than that with an iridium ruthenium electrode and an Sb-doped $SnO_2$/Ti electrode. After 60 minutes of reaction, the removal rates of CIP by the platinum-plated titanium electrode are 79.35% and 83.62%, respectively. This is mainly because the platinum-plated titanium electrode has a strong electrocatalytic effect and can generate a large amount of ·OH in the reaction system, thus promoting the degradation of CIP [40]. In addition, the platinum-plated titanium material has strong conductivity, electrocatalytic performance, and electrochemical stability. Therefore, the platinum-plated titanium electrode was chosen as the anode for the subsequent three-dimensional electron-Fenton reaction.

Fig. 5 (c); Fig. 5 (d) shows the effect of cathode types on CIP degradation. It was found that the degradation rate of CIP using a foam nickel electrode was 84.12% higher than that using activated carbon fiber electrodes and 17.28% higher than that using graphite electrode. The graphite on the electrode surface is easily detached when exposed to an oxidizing environment for an extended period [41]. In a prolonged oxidation environment, the graphite on the electrode surface is prone to fall off [41]. Therefore, based on the comprehensive analysis of the CIP removal effect of each elec- trode plate, foam nickel was selected as the cathode material for the subsequent three-dimensional electric Fenton reaction.

## 3.6. Analysis of CIP Degradation by Three-Dimensional Electric Fenton

It has been reported that biochar has oxidation-reduction activity and can be used as an electron shuttle to facilitate the $Fe^{3+}/Fe^{2+}$ cycle in the electric Fenton system [42]. At the same time, biochar has a high specific surface area and an abundant porous structure,

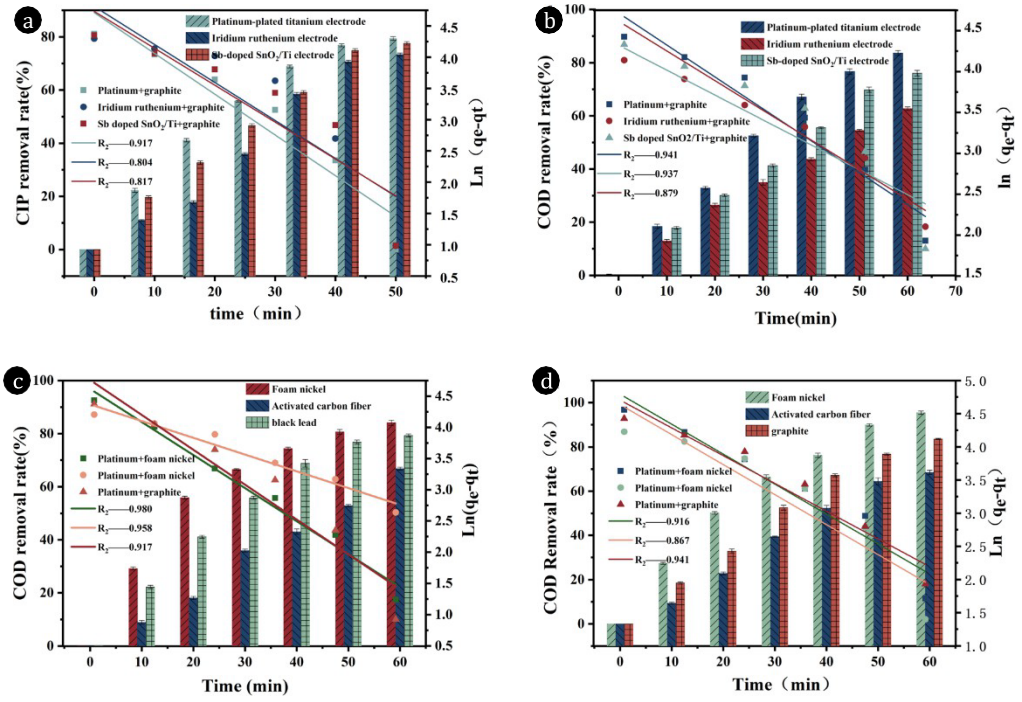


**Fig. 5.** Anode plate screening. (a) CIP removal rate (b) COD removal rate Cathode plate screening (c) CIP removal rate (d) COD removal rate.

which can provide enough active sites for electrochemical oxida- tion [43]. Given the advantages of biochar for electrochemical reactions and its high adsorption capacity, it shows promise to utilize biochar for adsorbing CIP during the electrochemical reaction in an electric Fenton system.

To demonstrate the capability of the electric Fenton system in decomposing CIP, this study employed the ultraviolet full-band scanning method. A platinum-plated titanium electrode was chos- en as the anode, and a foam nickel electrode was selected as the cathode for electric Fenton as a control for CIP degradation. The experimental results are shown in Fig. 6. It can be observed that the original solution exhibited strong absorption peaks at
276.5 nm and 332.5 nm, corresponding to the piperazine ring and quinolone ring of CIP, respectively. After 60 minutes of reaction, however, these two adsorption peaks were significantly weakened, indicating the breakdown of CIP in the system. Nevertheless, the absorption characteristic peaks of CIP still persisted. This indicates that the three-dimensional electric Fenton reaction did not entirely eliminate the chromophore of CIP. Instead, it generated inter- mediate compounds and small molecular substances.

To compare with the control experiment without biochar, the electric Fenton system with the addition of biochar was further investigated for CIP degradation and removal. In an external electric field, the particle electrode, such as biochar, can be polarized into countless microelectrodes. Particle electrodes carry opposite charges at both ends, thereby enhancing the effect of elec- tro-adsorption. In addition, the degradation of CIP in the BSJ electric Fenton system mainly involves direct discharge oxidation and indirect oxidation [44]. Direct oxidation occurs not only on the surface of anodic electrodes, similar to two-dimensional electrodes, but also on the surface of BSJ particle electrodes. According to Lu et al.'s research, in a three-dimensional electric Fenton system, active substances (·OH and·$O_2$) indirectly oxidize CIP. Therefore, the degradation of CIP by the electric Fenton system results from the direct oxidation of BSJ particle electrodes and the indirect oxidation of active substances in the electric Fenton system.

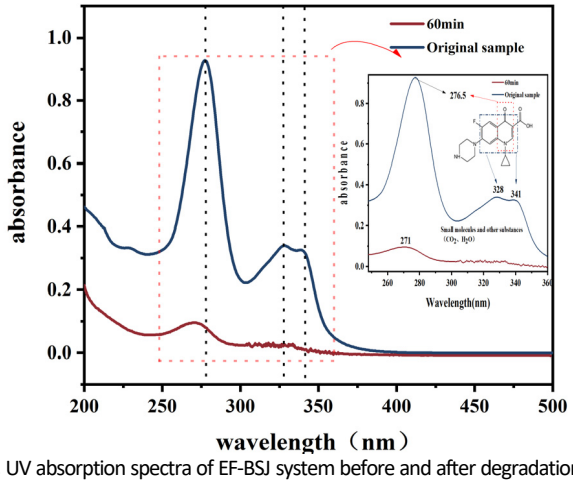


**Fig. 6.** UV absorption spectra of EF-BSJ system before and after degradation of CIP.

## 4. Conclusions

This study involved the production of biochar from the naturally lignin-rich porous material of *Jacaranda* fruit shell. The biochar was then integrated into a three-dimensional electric Fenton system to treat antibiotic wastewater. The experimental results indicated that the optimal carbonization temperature and time for BSJ are 800°C and 1 hour. Under the conditions of the experiment, the saturated adsorption capacity of BSJ for CIP is 6.89 mg/g. The maximum adsorption capacity of BSJ for methylene blue dye is 374.59 mg/g, and the maximum adsorption capacity for $Pb^{2+}$ in heavy metal is 58.47 mg/g. Biochar saturated with antibiotics was added to the three-dimensional electric Fenton system for antibiotic degradation. When the anode material is a platinum-plated titanium electrode and the cathode is a foam nickel electrode, the degradation rates of CIP and COD in the BSJ-/EF system are 84.12% and 95.48%, respectively. Finally, CIP is oxidized into small molecular substances by the electric Fenton system after being adsorbed by BSJ, which reduces the concentration of CIP in the system.

## Conflict-of-Interests Statement

The authors declare no competing interests.

## Acknowledgements

The study is supported by Sichuan Science and Technology Program (2019YJ0514).

## Author Contributions

G.H.L. (Professor) guided this paper. Y.Q.L. (Master's student) conceptualized, wrote, and revised the manuscript. Y.Q.L. (Professor) provided suggestions for the manuscript. H.Y.Q. (Associate Professor) provided suggestions for the manuscript. B.X. (Associate Professor) provided suggestions for the manuscript. Y.S. (Master's student) conducted all experiments. A.L.F. (Master's student) revised the manuscript. M.Z. (Master's student) wrote the manuscript.

## References

1. Van DX, Dewulf J, Van LH, Demeestere K. Fluoroquinolone antibiotics: An emerging class of environmental micropollutants. *Sci. Total Environ.* 2014;500-501:250-269. https://doi.org/10.1016/ j.scitotenv.2014.08.075.
2. Irina E, Marina T, Niina D. Degradation of levofloxacin in aqueous solutions by Fenton, ferrous ion-activated persulfate and combined Fenton/persulfate systems. *Chem. Eng. J.* 2015;279:452-462. https://doi.org/10.1016/j.cej.2015.05.054.
3. Ao XW, Liu WJ, Sun WJ, et al. Medium pressure UV-activated peroxymonosulfate for ciprofloxacin degradation: Kinetics, mechanism, and genotoxicity. *Chem. Eng. J.* 2018;345:87-97.

https://doi.org/10.1016/j.cej.2018.03.133
4. Duan XG, Sun HQ, Wang YX, Kang J, Wang SB. N-doping-in- duced nonradical reaction on single-walled carbon nanotubes for catalytic phenol oxidation. *ACS Catal.* 2015;5:553-559. https://doi.org/10.1021/cs5017613.
5. Li YC, Xing B, Ding Y, Han XH, Wang SR. A critical review of the production and advanced utilization of biochar via se- lective pyrolysis of lignocellulosic biomass. *Bioresour. Technol.* 2020;312:123614. https://doi.org/10.1016/j.biortech.2020.123614.
6. Li Y, Wang F, Miao YW, et al.A lignin-biochar with high oxy- gen-containing groups for adsorbing lead ion prepared by simul- taneous oxidization and carbonization. *Bioresour. Technol.* 2020;307:123165. https://doi.org/10.1016/j.biortech.2020.123165.
7. Chen YC, Liu JT, Zeng QB, et al.Preparation of Eucommia ulmoides lignin-based high-performance biochar containing sulfonic group: Synergistic pyrolysis mechanism and tetracy- cline hydrochloride adsorption. *Bioresour. Technol.* 2021;329: 124856. https://doi.org/ 10.1016/j.biortech.2021.124856.
8. Yaashikaa PR, Senthil kP, Varjani SJ, Saravanan A. Advances in production and application of biochar from lignocellulosic feedstocks for remediation of environmental pollutants. *Bioresour. Technol.* 2019;292:122030. https://doi.org/10.1016/ j.biortech.2019.122030.
9. Trevino CH, Juarez ALG, Mendoza CDI. Synthesis and adsorp- tion properties of activated carbons from biomass of Prunus domestica and Jacaranda mimosifolia for the removal of heavy metals and dyes from water. *Ind. Crops Prod.* 2013;42:315-323. https://doi.org/10.1016/j.indcrop.2012.05.029.
10. Yi YQ, Huang ZX, Lu BZ, et al. Magnetic biochar for environ- mental remediation: A review. *Bioresour. Technol.* 2020;298: 122468. https://doi.org/10.1016/j.biortech.2019.122468.
11. Siré SI, Brillas E, Oturan M, Rodrigo M, Panizza M. Electrochemical advanced oxidation processes: today and tomorrow. A review. *Environ. Sci. Pollut. Res.* 2014;21:8336- 8367. https://doi.org/10.1007/s11356-014-2783-1.
12. Acevedo GV, Rosales E, Puga A, Pazos M, Sanromán MA. Synthesis and use of efficient adsorbents under the principles of circular economy: Waste valorisation and electroadvanced oxidation process regeneration. *Sep. Purif. Technol.* 2020;242: 116796. https://doi.org/10.1016/j.seppur.2020.116796.
13. Chen YP, Yang LM, Chen JP, Zheng YM. Electrospun spongy zero-valent iron as excellent electro-Fenton catalyst for en- hanced sulfathiazole removal by a combination of adsorption and electro-catalytic oxidation. *J. Hazard. Mater.* 2019;371: 576-585. https://doi.org/10.1016/j.jhazmat.2019.03.043.
14. Zhang C, Jiang YH, Li YL, Hu ZX, Zhou L, Zhou MH. Three-di- mensional electrochemical process for wastewater treatment: A general review. *Chem. Eng. J.* 2013;228:455-467. https://doi. org/10.1016/j.cej.2013.05.033.
15. Ammar S, Oturan MA, Labiadh L, et al. Degradation of tyrosol by a novel electro-Fenton process using pyrite as heterogeneous source of iron catalyst. *Water Res.* 2015;74:77-87. https://doi. org/10.1016/j.watres.2015.02.006.
16. Segura Y, Martínez F, Melero JA. Effective pharmaceutical wastewater degradation by Fenton oxidation with zero-valent iron. *Appl. Catal., B.* 2013;136-137:64-69. https://doi.org/ 10.1016/j.apcatb.2013.01.036.

17. Zhao X, Li AZ , Mao R, Liu HJ, Qu JH. Electrochemical removal of haloacetic acids in a three-dimensional electrochemical re- actor with Pd-GAC particles as fixed filler and Pd-modified carbon paper as cathode. *Water Res.* 2014;51:134-143. https://doi.org/10.1016/j.watres.2013.12.028.
18. Hu J, Yang ST, Wang XK. Adsorption of Cu(II) on β-cyclodextrin modified multiwall carbon nanotube/iron oxides in the ab- sence/presence of fulvic acid. *J. Chem. Technol. Biotechnol.* 2012;87:673-681. https://doi.org/10.1002/jctb.2764.
19. Shokoofeh G, Alireza A, Alireza B. Synthesis and Characterization of Nanoporous Carbon Materials; The Effect of Surfactant Concentrations and Salts. *E-J. Chem.* 2018;8:8. https://doi.org/10.1155/2011/967319.
20. Sun L, Chen DM, Wan SG, Yu ZB. Performance, kinetics, and equilibrium of methylene blue adsorption on biochar derived from eucalyptus saw dust modified with citric, tartaric, and acetic acids. *Bioresour. Technol.* 2015;198:300-308. https://doi. org/10.1016/j.biortech.2015.09.026.
21. Wang Q, Jiao GJ, Liu HP, Bai JR, Li SH. Variation of the pore sstructure during microwave pyrolysis of oil shale. *Oil Shale.* 2010;27:135-146. https://doi.org/10.3176/oil.2010.2.04.
22. Li HB, Dong XL, da Silva EB, de Oliveira LM, Chen YS, Ma LNQ. Mechanisms of metal sorption by biochars: Biochar char- acteristics and modifications. *Chemosphere.* 2017;78:466-478. https://doi.org/10.1016/j.chemosphere.2017.03.072.
23. Qambrani NA, Rahman MM, Won S. Biochar properties and eco-friendly applications for climate change mitigation, waste management, and wastewater treatment: A review. *Renew. Sustain. Energy Rev.* 2017;79:255-273. https://doi.org/10.1016/ j.rser.2017.05.057.
24. Yu BM, Gele A, Wang LP. Iron oxide/lignin-based hollow carbon nanofibers nanocomposite as an application electrode materials for supercapacitors. *Int. J. Biol. Macromol.* 2018;118:478-484. https://doi.org/10.1016/j.ijbiomac.2018.06.088.
25. Mahmoud ME, Nabil GM, El-Mallah NM, Bassiouny HI, Kumar S, Abdel-Fattah TM. Kinetics, isotherm, and thermodynamic studies of the adsorption of reactive red 195 A dye from water by modified Switchgrass Biochar adsorbent. *J. Ind. Eng. Chem.* 2016;37:156- 167. https://doi.org/10.1016/j.jiec.2016.03.020.
26. Zhang JH, Huang B, Chen L, Yang L, Li W, Luo ZX. Characteristics of biochar produced from yak manure at differ- ent pyrolysis temperatures and its effects on the yield and growth of highland barley. *Chem. Speciation Bioavailability.* 2018;30:67. https://doi.org/10.1080/09542299.2018.1487774.
27. Song WP, Guo MX. Quality variations of poultry litter biochar generated at different pyrolysis temperatures. *J. Anal. Appl. Pyrolysis.* 2012;94:138-145. https://doi.org/10.1016/j.jaap.2011. 11.018.
28. Chun Y, Sheng GY, Chiou CT, Xing BS. Compositions and sorptive properties of crop residue-derived chars. *Environ. Sci. Technol.* 2004;38:4649-4655. https://doi.org/10.1021/es035034w.
29. Zeng ZW, Tian SR, Liu YG, et al. Comparative study of rice husk biochars for aqueous antibiotics removal. *J. Chem. Technol. Biotechnol.* 2018;93:1075-1084. https://doi.org/10.1002/jctb.5464.
30. Asadi SZ, Galangash MM, Younesi H, Nowrouzi M. The feasi- bility of cost-effective manufacturing activated carbon derived from walnut shells for large-scale CO2 capture. *Environ. Sci.*

*Pollut. Res.* 2019;26:26542-26552. https://doi.org/10.1007/s11356- 019-05842-3.
31. Zhang J, Liu J, Liu RL. Effects of pyrolysis temperature and heating time on biochar obtained from the pyrolysis of straw and lignosulfonate. *Bioresour. Technol.* 2015;176: 288-291. https://doi.org/10.1016/j.biortech.2014.11.011.
32. Jie Y, Paterson N, Blamey J, Millan M. Cellulose, xylan and lignin interactions during pyrolysis of lignocellulosic biomass. *Fuel.* 2017;191:140-149. https://doi.org/10.1016/j.fuel.2016.11.057.
33. Wu YC, Chen YZ, Zeng Y, Li C, Qiu RH, Liu WD. Photo-curing preparation of biobased underwater adhesives with hydro- phobic chain-ring interlace structure for protecting adhesion. *Appl. Mater. Today.* 2022;27. https://doi.org/10.1016/j.apmt. 2022.101436.
34. Chang JL, Ma JC, Ma QL, et al. Adsorption of methylene blue onto Fe3O4/activated montmorillonite nanocomposite. *Appl. Clay Sci.* 2016;119:132-140. https://doi.org/10.1016/j.clay.2015. 06.038.
35. Rangabhashiyam S, Balasubramanian P. The potential of ligno- cellulosic biomass precursors for biochar production: Performance, mechanism and wastewater application—A review. *Ind. Crops Prod.* 2019;128:405-423. https://doi.org/10. 1016/j.indcrop.2018.11.041.
36. Qiu BB, Tao XD, Wang H, Li WK, Ding X, Chu HQ. Biochar as a low-cost adsorbent for aqueous heavy metal removal: A review. *J. Anal. Appl. Pyrolysis.* 2021;155:105081. https://do- i.org/10.1016/j.jaap.2021.105081.
37. Gupta S, Sireesha S, Sreedhar I, Patel CM, Anitha KL. Latest trends in heavy metal removal from wastewater by biochar based sorbents. *J. Water Process Eng.* 2020;38:101561. https://doi.org/10.1016/j.jwpe.2020.101561.

38. Hyun MJ, Seunghyun Y, Yong KC, Sunkyu P, Eunsung K. Adsorption isotherm, kinetic modeling and mechanism of tetra- cycline on Pinus taeda_derived activated biochar. *Bioresour. Technol.* 2018;259:24-31. https://doi.org/10.1016/j.biortech.2018.03.013.
39. Li XY, Liu TLX, Han X, Li YL, Ma XL. Removal of heavy metals lead and ciprofloxacin from farm wastewater using pea- nut shell biochar. *Environ. Technol. Innovation.* 2023;30: 103121. https://doi.org/10.1016/j.eti.2023.103121.
40. Chen L, Hoff S, Cai L, Koziel J, Zelle B. Evaluation of wood chip-based biofilters to reduce odor, hydrogen sulfide, and ammonia from swine barn ventilation air. *J. Air Waste Manage. Assoc.* 2009;59:520-530. https://doi.org/10.3155/1047-3289.59.5.520.
41. Ángel FS, Gabriela L, Marta P, Emilio R, Maria ÁS. Bridging the gap to hydrochar production and its application into frame- works of bioenergy, environmental and biocatalysis areas. *Bioresour. Technol.* 2021;320:124399. https://doi.org/10.1016/j.biortech.2020.124399.
42. Laura K, Marco K, Markus K, Michael S. Redox Properties of Plant Biomass-Derived Black Carbon (Biochar). *Environ. Sci. Technol.* 2014;48:5601-5611. https://doi.org/10.1021/es500906d.
43. Wang JL, Wang SZ. Preparation, modification and environ- mental application of biochar: A review. *J. Cleaner Prod.* 2019;227:1002-1022. https://doi.org/10.1016/j.jclepro.2019.04.282.
44. Lu CP, Wei GT, Ba JS, et al. Three-dimensional electro-Fenton degradation of ciprofloxacin catalyzed by CuO doped red mud particle electrodes: Electrodes preparation, kinetics and mechanism. *J. Environ. Chem. Eng.* 2022;10:2. https://doi.org/10.1016/j.jece.2022.107151.